

First measurements of betatron radiation at FLAME laser facility



A. Curcio^{a,b,*}, M. Anania^a, F. Bisesto^{a,b}, E. Chiadroni^a, A. Cianchi^a, M. Ferrario^a, F. Filippi^{a,b}, D. Giulietti^c, A. Marocchino^a, F. Mira^b, M. Petrarca^d, V. Shpakov^a, A. Zigler^{a,e}

^a INFN-LNF, via Enrico Fermi 40, 00044 Frascati (Rome), Italy

^b Department of Physics, "Sapienza" University of Rome, Piazzale A. Moro 2, I-00185 Rome, Italy

^c Physics Department of the University and INFN, Largo Bruno Pontecorvo 3, 56127 Pisa, Italy

^d Department of Basic and Applied Sciences for Engineering (SBAl) and INFN-Roma1, "Sapienza" University of Rome, Via A. Scarpa 14, 00161 Rome, Italy

^e Racah Institute of Physics, Hebrew University, Jerusalem 91904, Israel

ARTICLE INFO

Article history:

Received 6 December 2016

Received in revised form 14 February 2017

Accepted 21 March 2017

Available online 31 March 2017

Keywords:

Blowout regime

Betatron radiation

X-rays

ABSTRACT

The first results on betatron radiation obtained in laser-plasma acceleration experiments at the FLAME laser facility are presented. The diagnostic apparatus for the X-ray detection available at the facility is described together with the experimental setup for the generation of betatron radiation.

© 2017 Elsevier B.V. All rights reserved.

1. Introduction

The betatron radiation is the wiggler-like synchrotron radiation [1–14] emitted by electrons accelerated in laser-plasma wakefields [16]. In the strongly non-linear regime, i.e. at laser extremely relativistic intensities, the wakefield accelerating structure for the electrons is bubble-like [17,18] and the electrons are self-injected from the rear of the bubble inside the accelerating and focusing region, completely depleted from electrons by the strong ponderomotive laser potential at its passage through the underdense plasma. Here we present the first results on betatron X-ray detection performed at the FLAME laser facility [19–21] of the National Laboratories of Frascati of INFN. The X-ray diagnostics available at the facility are briefly described and finally it is shown how they have been strategically used for the detection of betatron radiation in self-injection laser-plasma acceleration experiments.

2. X-ray diagnostics at FLAME facility

The hard X-ray spectrometer (Fig. 1) available at the FLAME laser facility is the CdTe (model AMPTEK X-123CdTe) [22], having an active area of 9 mm², a 1000 μm semiconductor thickness and a 100 μm Be window. The detector is mounted on a thermoelectric

cooler for reducing the electronic noise. It combines, in a single package, the CdTe drift X-ray detector and preamplifier, the digital pulse processor (AMPTEK DP5) and MCA, and the Power Supply (AMPTEK PC5). It works in an energy range of 5 ÷ 150 keV with energy resolution less than 1.2 keV FWHM at 122 keV.

The soft X-ray detector at the facility is the Andor DX 434 BR-DD (Fig. 2), where BR-DD stays for Back illuminated CCD, Deep Depletion NIR AR coating. The active pixels are 1024 × 256, the pixel size is 26 × 26 μm, the image area is 26.6 × 6.7 mm², it is vacuum compatible down to 10^{−5} millibar and below and the maximum cooling is about −100°.

Both the CdTe spectrometer and the CCD-X camera utilized as spectrometer can work only with low X-ray fluxes, i.e. in single photon counting. The X-ray scintillator [23] (Fig. 3) foil is based on Ti-doped CsI single crystals, the pixel size is ~50 μm while the foil area is 10 cm².

The X-ray scintillator is positioned before the X-ray spectrometer and the X-ray filters because it can work at high-flux. In this way the scintillator allows the measurement of spatial distribution of the X-ray radiation simultaneously to the spectrum detection, which is performed at low flux after damping the radiation (Fig. 5).

3. Experimental results

A self-injection experimental campaign was performed at the SPARC-LAB test facility (INFN-LNF) by using the laser FLAME. The main pulse characteristics were changed according to various tests

* Corresponding author at: Department of Physics, "Sapienza" University of Rome, Piazzale A. Moro 2, I-00185 Rome, Italy.

E-mail address: curcioalexander@gmail.com (A. Curcio).

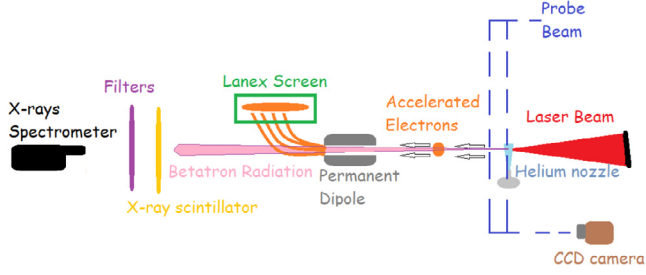


Fig. 5. Experimental setup: the FLAME laser beam is focused about one hundred microns before the He gas-jet. Electrons are accelerated in the blowout regime over a distance ranging 1–2 mm, according to the diameter of the gas-nozzle and of the plasma density. The permanent dipole ($\lesssim 1$ T) coupled with a LANEX screen allows the measurement of the electron energy spectrum. The X-ray betatron radiation, directed in the same direction of the impinging laser, crosses a X-ray scintillator in order to detect the spatial distribution of the radiation and then it arrives at the X-ray spectrometer, where the photon spectrum is detected. Filters of kapton and aluminium are exploited on the light-line in order to damp the X-ray radiation and screen the residual laser light. The Probe beam is coupled to a Mach-Zender interferometer in order to retrieve the electron plasma density of the laser-produced plasma channel.

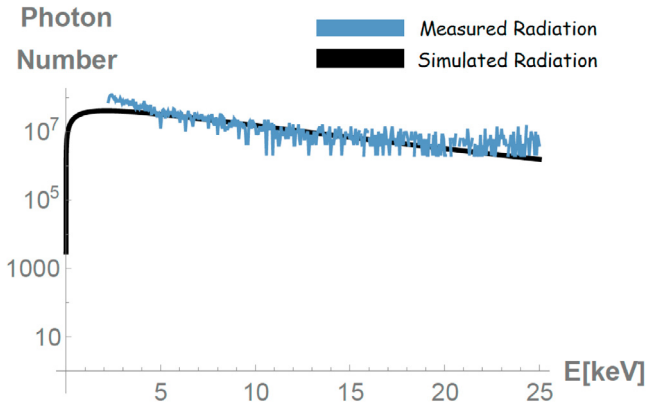


Fig. 6. Betatron radiation spectrum detected by the CdTe spectrometer. Laser, plasma and electron parameters: energy per pulse $E_L = 1.5$ J, pulse duration $\tau = 35$ fs, focus rms radius $\sigma_r \sim 5$ μ m. Electron plasma density $n_e \sim 6 \pm 1 \times 10^{18}$ cm $^{-3}$, electron mean energy 200 MeV, energy spread 30%, electron beam divergence 12 mrad, bunch charge 20 pC. The acceleration length was 1 mm.

polyenergetic electron beams, with energies and energy spreads consistent both with the measurements and with the expression given in Ref. [18], from which the maximum electron energy gain in the bubble regime is $2m_e c^2 a_0 \omega_0^2 / 3\omega_p^2$, where m_e is the electron mass, c is the speed of light in vacuum, ω_0 and ω_p the laser pulsation and the plasma frequency respectively.

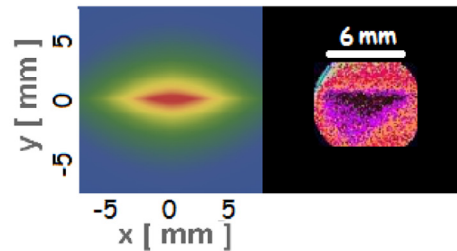
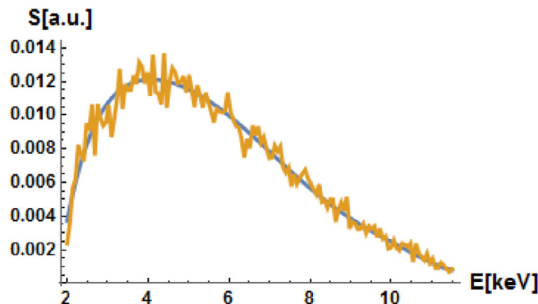


Fig. 7. Betatron radiation spectrum detected by the CCD-X camera working in single photon counting (left) and betatron radiation spatial distribution (right, simulation and measurement) relative to the same shot detected through the X-ray scintillator positioned in front of the X-ray camera. Laser, plasma and electron parameters: energy per pulse $E_L = 1$ J, pulse duration $\tau = 30$ fs, focus rms radius $\sigma_r \sim 5$ μ m. Electron plasma density $n_e \sim 0.9 \pm 0.1 \times 10^{19}$ cm $^{-3}$, electron mean energy ~ 300 MeV, energy spread 20%, electron beam divergence 5 mrad, bunch charge 5 pC. The acceleration length was 1.1 mm.

The betatron radiation emitted by the accelerated electrons during the interaction of the high-intensity laser with the He plasma was detected with three different detectors for different configurations of laser intensity and electron plasma density. It was detected with a CdTe X-ray spectrometer, with a calibrated CCD-X camera and with a X-ray scintillator. The spectrometers were positioned at 0.7 m from the interaction point, the CCD-X camera was cooled down to -30 $^{\circ}$ C and shielded by a lead cage. The goal was that of measuring simultaneously the spatial distribution of the radiation with the X-ray scintillator and the spectrum in single photon counting mode with the spectrometers. The X-ray scintillator was positioned in front of the CCD-X at 0.5 m from the interaction point. The betatron X-ray flux had to cross an overall absorbing thickness constituted by a 280 μ m kapton window, a 200 μ m X-ray scintillator screen and 1 μ m Al filter to screen the residual infrared light on the X-ray spectrometers.

The CdTe was used when betatron radiation extending towards hard X-rays above 10 keV was expected, while when soft X-ray radiation was expected from simulations based on the actual values of the laser intensity and of the electron plasma density, the CCD-X camera was adopted for the spectral detection. In Fig. 6 the betatron spectrum detected by the CdTe spectrometer is reported together with the comparison to the simulation. The simulation of the betatron spectrum was performed by using the fields resulting from 3D PIC simulations, and tracking 10^4 particles over a length given by the measured L_{acc} . The betatron spectrum formula used for the calculations is [28,29]:

$$\frac{dI}{dE} = -\frac{2\alpha E}{\sqrt{\pi} \hbar} \int_0^{L_{acc}/c} \frac{dt}{\gamma^2(t)} \left[\frac{\Phi(u)}{u} + \frac{1}{2} \int_{-\infty}^{\infty} du \Phi(u) \right] \quad (1)$$

where $\Phi(u)$ is the Airy function of first kind where we defined:

$$u = \left(\frac{2E}{\hbar c k_p^2 x(t) \gamma^2(t)} \right) \quad (2)$$

dI is the differential radiated energy, α the fine structure constant, $x(t)$ is the transverse coordinate of the electron undergoing betatron oscillations, \hbar the Planck constant, $k_p = \omega_p/c$ the plasma wavenumber, γ the electron Lorentz factor and E the energy of the radiated photon. The measured electron energy spectrum ranged as 200–350 MeV with an energy spread $2\sigma_\gamma/\gamma_0 \sim 20$ –30%. We measured the higher electron energies when the density was around 8×10^{18} cm $^{-3}$. This is explainable by the fact that for our laser intensity the dephasing length $4c\sqrt{a_0}\omega_0^2/3\omega_p^2$ was well matched to the measured acceleration length for densities around 8×10^{18} cm $^{-3}$. Below this value, the dephasing length was much longer than the acceleration length, therefore the measured electron energy gain was smaller. Also it's worth noting that the

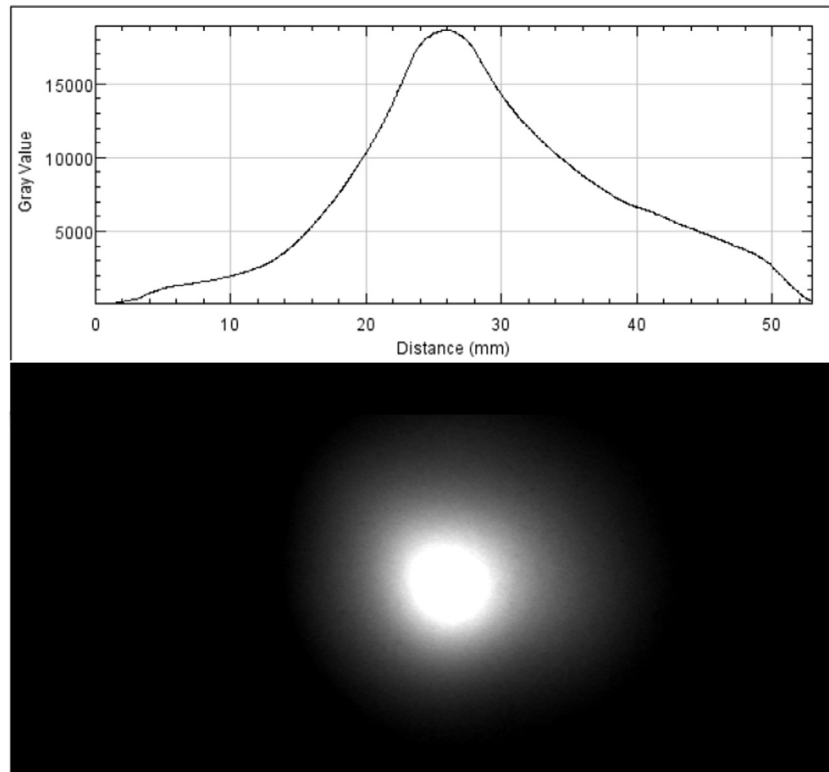


Fig. 8. Charge profile detected with the Imaging Plate after 3 meters from the interaction point. The total charge in this case was 5 pC.

betatron spectra we show in Fig. 6 and 7 differ from each other about the spectral extension. Actually the parameter which determines the spectral extension is the critical energy [1], which increases with the electron energy and with the beam size. Therefore even if the energy of the electron beam in the case of Fig. 7 is bigger than that corresponding to Fig. 6, we got much smaller beam size (well below the micron scale [14]) in the first case than in the second (the size of the bunches here was on the micron scale, measured with the technique of Ref [14]). The net effect was that the critical energy was higher at smaller densities, because for our laser intensities we found an optimum matching of the self-injected electron bunch for densities around $8 \times 10^{18} \text{ cm}^{-3}$. The betatron radiation spectrum detected with the CCD-X camera and the spatial distribution of the radiation measured with the X-ray scintillator are shown in Fig. 7. The spatial distribution was asymmetric in the x-direction, the direction of the laser polarization, because for the plasma density $9 \pm 1 \times 10^{18} \text{ cm}^{-3}$ the dephasing length was slightly smaller than the measured acceleration length and the tail of the laser penetrated significantly the bubble. In this condition the tail of the laser pulse can resonantly interact with the electrons close to the dephasing point, determining strong oscillations in the direction of the polarization and strong emission of radiation with typically asymmetric distributions elongated in the oscillation direction (see also Fig. 4). We simulated the distribution of the radiation by using the radiation distribution formula in Ref. [28] and the analytical trajectories of Ref. [30] for laser-driven betatron oscillations. This regime of interaction is also called Direct Laser Acceleration because the particles interacting with the laser tail acquire a significant relativistic mass. The condition for the DLA is $R \sim c\tau$, where the bubble radius is $R = 2\sqrt{a_0}/k_p$ and τ is the rms duration of the laser pulse. Both the simulation and the measurement of betatron spatial distribution gave asymmetric distributions in the polarization plane of the laser and with fully comparable divergences. The charge was measured by an Imaging Plate put 3 meters

after the interaction point. The Gray Level image is shown in Fig. 8. The Gray Level value was converted in PSL via the calibration presented in the work [31]. Then by the characterization of the Imaging Plates done in the work [32] where the PSL/electron values are reported for different electron energies, we measured charges typically in the range 1–20 pC.

4. Conclusions

The first measurements of betatron radiation in laser-plasma acceleration experiments performed at the National Laboratories of Frascati of the INFN have been shown and the X-ray available diagnostics at the FLAME laser facility have been described. The key role of betatron radiation in the laser plasma acceleration activity at FLAME will be that to provide information about the electron beam emittance inside the plasma accelerating structure.

Acknowledgements

This work has been partially supported by the EU Commission in the Seventh Framework Program, Grant Agreement 312453 EuCard-2, by the Italian Ministry of Research in the framework of FIRB - Fondo per gli Investimenti della Ricerca di Base, Project No. RBFR12NK5K.

References

- [1] A. Rousse et al., *Phys. Rev. Lett.* 93 (2004) 135005.
- [2] S. Wang et al., *Phys. Rev. Lett.* 88 (13) (2002) 135004.
- [3] S. Kneip et al., *Appl. Phys. Lett.* 99 (9) (2011) 093701.
- [4] S. Fourmaux et al., *Opt. Lett.* 36 (13) (2011) 2426–2428.
- [5] S. Kneip et al., *Nat. Phys.* 6 (12) (2010) 980–983.
- [6] M. Mo et al., *Rev. Sci. Instrum.* 84 (12) (2013) 123106.
- [7] S. Kneip et al., *Phys. Rev. ST Accel. Beams* 15 (2) (2012) 021302.
- [8] G.R. Plateau et al., *Phys. Rev. Lett.* 109 (6) (2012) 064802.
- [9] M. Schnell et al., *Phys. Rev. Lett.* 108 (7) (2012) 075001.

- [10] A. Kühler et al., Nucl. Instrum. Methods A 829 (2016).
- [11] F. Albert et al., Physical Review E 77 (5) (2008) 056402.
- [12] D.B. Thorn et al., Rev. Sci. Instrum. 81 (2010) 10E325.
- [13] S. Fourmaux et al., New J. Phys. 13 (3) (2011) 033017.
- [14] A. Curcio et al., Phys. Rev. ST Accel. Beams 20 (1) (2017) 012801.
- [15] T. Tajima, J.M. Dawson, Phys. Rev. Lett. 43 (1979) 267.
- [16] A. Pukhov et al., Plasma Phys. Controlled Fusion 46 (2004) B179.
- [17] W. Lu et al., Phys. Rev. ST Accel. Beams 10 (2007) 061301.
- [18] M. Ferrario et al., Nucl. Instrum. Meth. B 183–188 (2013).
- [19] D. Giulietti, Journal of Physics: Conference Series (Vol. 508, No. 1, p. 012001). IOP Publishing, 2014.
- [20] L.A. Gizzi et al., Appl. Sci. 3 (3) (2013) 559–580.
- [21] A. Curcio et al., 2016 JINST 11C05011.
- [22] M. Nikl, Meas. Sci. Technol. 17 (2006) R37–R54.
- [23] S. Sinigardi et al., 2016, DOI: 10.5281/zenodo.49553.
- [24] C. Benedetti et al., IEEE Trans. Plasma Sci. 36 (4) (2008) 1790–1798.
- [25] P. Londrillo et al., Nucl. Instrum. Methods A 620 (1) (2010) 28–35.
- [26] A. Marocchino et al., Efficient modeling of plasma wakefield acceleration in quasi-non-linear-regimes with the hybrid code Architect, Nucl. Instrum. Methods Phys. Res. Sect. A: Accelerators, Spectrometers, Detectors Associated Equip. 829 (2016) 386–391.
- [27] A. Curcio, D. Giulietti, Nucl. Instrum. Methods B 355 (2015) 214–216.
- [28] A. Curcio et al., Phys. Plasmas 24 (2) (2017) 023104.
- [29] A. Curcio et al., J. Plasma Phys. 81 (05) (2016) 495810513.
- [30] F. Ingenito et al., proceedings of Plasma Physics by Laser and Applications (PPLA 2015), ENEA Research Centre, Frascati, Italy, 5–7 October 2015, 2016 JINST 11 C05012.
- [31] Nakanii et al., Journal of Physics: Conference Series 112 (3) (2008), IOP Publishing.